

DESIGN AND DEVELOPMENT OF ELECTRIC SUBMERSIBLE PUMPS FOR LARGE CAPACITIES

by

Andreas Hosøy

Project Engineer

Sigve Gjerstad

Project Engineer

Jostein Smaamo

Project Engineer

and

Erik Torbergsen

Manager

Development Department

Frank Mohn Flatøy AS

Oil & Gas Division

Frekhaug, Norway



Andreas Hosøy is Project Engineer in the Development Department at Frank Mohn Flatøy AS, Oil & Gas Division, in Frekhaug, Norway. The company produces high energy pumping systems for the oil and gas industry. Mr. Hosøy joined the company in 2001 and works with general pump design and fluid mechanics.

Mr. Hosøy received his B.Eng. degree (Mechanical Engineering, 1997) from Bergen College of Engineering and his

M.Sc. degree (Mechanical Engineering, 1999) at The Norwegian University of Science and Technology.



Sigve Gjerstad is Project Engineer in the Development Department at Frank Mohn Flatøy AS, Oil & Gas Division, in Frekhaug, Norway. He joined the company in 2001 and works with general pump design and fluid mechanics.

Mr. Gjerstad received his B.Eng. degree (Mechanical Engineering, 1999) from the University of Newcastle, United Kingdom, and his M.Phil. degree (Mechanical Engineering, 2000) at Cambridge University.

Jostein Smaamo is Project Engineer in the Development Department at Frank Mohn Flatøy AS, Oil & Gas Division, in Frekhaug, Norway. He joined the company in 1998 and works with multidiscipline pump design with special focus on mechanical engineering.

Mr. Smaamo received his M.Sc. degree (Mechanical Engineering, 1992) from the University of Trondheim in Norway.

ABSTRACT

A submerged electric (SE) pump has been designed and analyzed for high flow applications. The challenges when designing a high power density SE pump are torsional and lateral dynamics and hydraulic stability. The case discussed in this paper is a single-stage pump rated for 7000 m³/h (31,000 gpm) with a mixed flow impeller and differential head of 65 m (213 ft). The increased flow design means that the impeller/motor inertia ratio increases compared to smaller designs. It is therefore important to review the torsional vibrations during start up when having direct online start. In this case the fundamental torsional critical was much higher than the main excitational frequency during start up, hence the response can be regarded as quasistatic. The main challenge with the lateral analysis was related to rotordynamic coefficients for the fluid filled clearances in the motor and impeller. The first bending mode was related to the motor itself, but with satisfactory separation margin from the operational speed. In addition, the response was highly damped. The impeller/diffuser interaction was analyzed with regard to flow stability. The diffuser can be a source for rotating stall that again can affect both vibrations and performance. Numerical flow simulations (computational fluid dynamics, CFD) were used to analyze the performance and flow at off-design. No sign of propagating recirculation around the circumference was detected. Additionally, casing/bearing house vibration analysis showed low vibration values and stable blade passing frequencies, confirming no blade-stall interactions and corresponding diffuser instability in the flow domain of interest.

INTRODUCTION

The market for submerged electric (SE) pumps with large capacities has increased over the last few years. Offshore oil and gas production, liquid natural gas (LNG) production, and floating production vessels (FPSO) with limited space available, all require significant amounts of process cooling water. Typical capacities for these pumps can be 5000 to 18,000 m³/h (22,000 to 79,300 gpm). SE pumps have been used for seawater applications in the oil and gas industry for many years. This paper describes the challenges involved in developing SE pumps for large capacities. It is directed

to oil and gas production and operational companies working with large capacity pumps.

The submerged electric pump is a vertical, close-coupled end-suction centrifugal pump with one or two stages. A 3D computer-aided design (CAD) model and a picture is shown in Figure 1 for the actual pump discussed in this paper. The suction inlet of the SE pump is the lowest point of the pump assembly. The motor for these pumps is a high voltage induction motor with supply frequency 50 or 60 Hz, two- to eight-poled with typical ratings from 500 kW to 3000 kW (670 to 4023 hp). The rotor is supported with rolling element bearings for both radial and axial thrust. The electric motor is filled and pressurized with oil. All bearings and the mechanical seal are lubricated and cooled by the forced oil circulation, supplied via three pipes as shown in Figure 1. These pipes also function as conductors for the electric motor, that is, no external cables are needed for the power supply. Both direct online start and variable frequency drives are applied but the most common configuration is a direct start up of the pump. The pump impeller(s) deliver into the outer shell of the pump housing, concentric with the motor housing. The diffuser design is based on axial guide vanes. The whole pump head with the integrated motor is completely submerged in water, at a sufficient depth to ensure satisfactory suction performance.

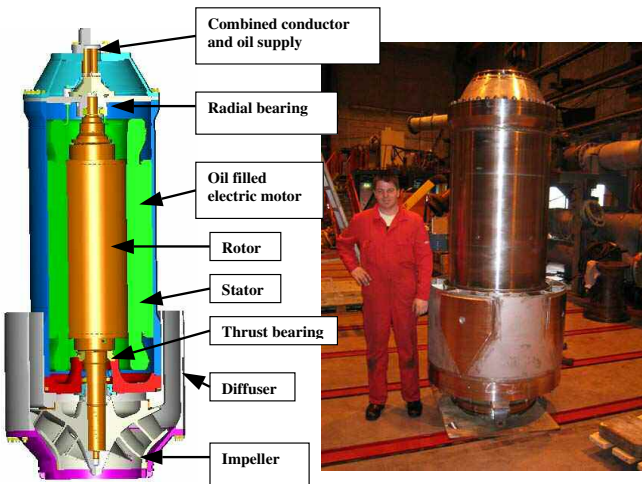


Figure 1. Sectional 3D CAD Model of the Actual High Capacity SE Pump (Left) and Picture of the Submersible Pump Discussed in This Paper (Right).

The design discussed in this paper is based on a demand for compact submerged pumps with high power densities and large capacities. It describes the development of a single-stage pump with flow rate of up to 11,000 m³/hr (48,400 gpm) and differential head 40 to 80 meters (131 to 262 ft). But as will be discussed, several technical challenges are important to discuss when extending SE pumps to larger capacities. For the design discussed in this paper, Table 1 shows the main design parameters and corresponding overall dimensions.

Table 1. Main Design Parameters for Actual Submerged Pump.

Design parameters and overall dimensions	Design data
Rated capacity Q [m ³ /h]	7000 (31000 gpm)
Rated head H [mlc]	65 (213 ft)
Process fluid	Sea water
NPSH r (3%) [mlc]	11 (36 ft)
Driver	6 pole induction motor
Shaft speed Ω_n [rpm]	985
Line frequency [Hz]	50

MAIN DESIGN CHALLENGES

The main design challenges in developing large submerged electric pumps are rotordynamic behavior (both lateral and torsional vibrations) and hydraulic design of impeller and diffuser. Increasing flow often means reduced speed and a relatively large impeller compared to the electric motor, hence, the impeller/motor inertia ratio will generally increase. For direct start up applications it is therefore important to focus on the transient impact torques. These torques can lead to large transient torsional vibrations during start up. The lateral vibrations are also important due to long life operation. Submerged pumps usually show vibration levels much lower than API limits, typically 50 percent. Low vibration levels should be kept when increasing the flow. Hydraulic design of impeller and diffuser is important, not only for achieving the right performance, but for obtaining a design that is hydraulically stable also at off-design conditions.

TRANSIENT TORSIONAL ANALYSIS

The motor transient oil filled “air gap” torque occurs at each direct start up from standstill. Induction motors having direct online start can excite significant torque pulsations during start up, typically three to five times the rated torque. The transient torques will be reduced and disappear when speed increases. For the type and size of motors analyzed here, this will typically happen after 200 to 400 ms. The exact alternating air-gap torque as a function of speed is difficult to model. However, the most important component is the peak exciting torque and frequency.

The transient torque in the “air gap” can be derived from the following general equation. For worst case loading, the rotational frequency of the rotor $\Omega_n = 0$.

$$\frac{T_{transient}(t)}{T_N} = \sum_i \left[\left(\frac{T_i}{T_N} \right) \cdot e^{-t/\tau_i} \cdot \sin \left(2 \cdot \pi \cdot f_{Ri} \cdot t + \phi_i \frac{2 \cdot \pi}{360} \right) \right] \quad (1)$$

where:

- (T_i/T_N) = Partial torque amplification (T_N = rated torque) [-]
- τ_i = Time constant [1/sec]
- f_{Ri} = Frequency content (zero or line frequency) [Hz]
- ϕ_i = Phase angle [degree]

In the above equation i = 1 to 4 and represents partial components in the transient model, comprising four components: one constant term, one lightly damped sinusoidal harmonic term, one second order highly damped term, and one first order highly damped term.

The technical data for the electrical induction motor applied here is shown in Table 2.

Table 2. Electric Motor Design Data at System Voltage U_N = 100 Percent.

Description of data	Data
Rated power output P _N [kW]	1650
Rated voltage U _N [V]	6000
Line frequency f _N [Hz]	50
Running speed Ω_N [rpm]/[Hz]	985/16.4
Driver and shaft polar moment of inertia I _{pdriver} [kgm ²]	20.5
Impeller load polar moment of inertia I _{pload} [kgm ²]	27.5

When superposing the terms in Equation (1) and combining this torque with the actual average start up torque from zero to rated speed, the simplified representation as shown in Figure 2 can be used in analyzing the torsional behavior. The time from zero to full speed is approximately 600 ms at 100 percent system voltage.

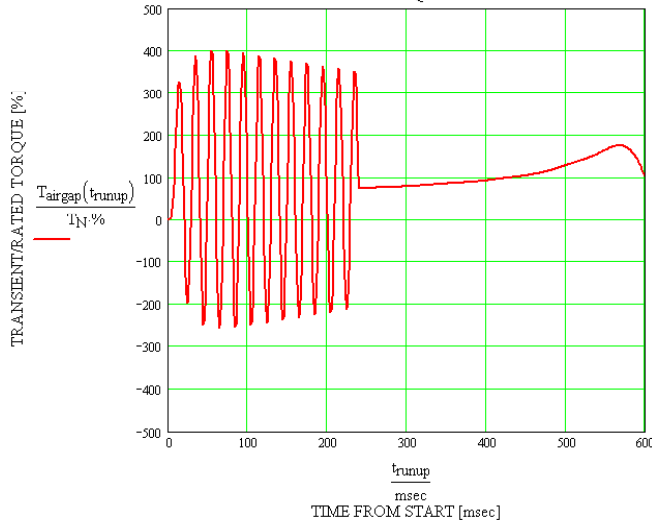


Figure 2. Simplified Model of the Motor “Air-Gap” Torque Model During Startup from Zero Speed to Steady-State Running Speed ($\Omega = 985 \text{ RPM}$).

The torsional dynamic stability of the large SE pump has been analyzed based on the above assumptions, giving a fundamental eigenvalue of 111 Hz, which is well above the highest (transient) excitation frequency of 50 Hz. The shaft response will therefore be so-called quasistatic (subcritical). The maximum shaft response torque during start up was calculated to be approximately 2.7 times the rated motor torque. This response torque has to be considered when designing the shaft and shaft/impeller connections.

Because of the alternating impact torques at start up, the impeller/shaft connection may be critical with respect to overload and damage, dependent on the chosen design. For these pumps, it is company standard to apply a taper/shrink fit between the large impeller and the shaft in order to ensure sufficient fit and avoid any fretting/fatigue problems often observed in key fitted designs.

LATERAL ROTORDYNAMIC ANALYSIS

The rotordynamic model is typically made up of the following main input data: wear ring seal stiffnesses, impeller rotordynamic coefficients with special focus on added mass, bearing coefficients, the oil filled motor dynamic coefficients and motor “air gap” magnetic elasticity. The challenge is to identify the dynamic interactions and specify the stiffnesses, damping, and added mass coefficients. For the actual case, the model is shown in Figure 3. The analysis was carried out using a commercially available program based on the transfer matrix method.

SE pump mode shapes are generally characterized by a high critical damping ratio and that the overhung impeller mode damped eigenvalue is well above the synchronous running speed, i.e., the SE pump will normally run subcritical, despite the large impeller fluid added mass typical for these pumps. To ensure that this also was the case when increasing the size of the pump, detailed analyses were carried out. This included a parameter study of the impeller rotordynamic coefficients on the global rotordynamic behavior, based on available published coefficients and inhouse developed coefficients from forced whirling experiments.

Rotor/Stator Clearance Interactions

Typical for the submerged motor is the significant added mass from fluid acting on the rotor, often described as the Stokes added mass, as presented by Black (1979). The added mass is inversely proportional to the clearance to radius ratio, $\sim 1/(C_r/R)$, and this relation is valid for $C_r/R \ll 1$.

The tangential velocity in the clearance also introduces negative stiffness effects, due to the inertia of the fluid. This is sometimes

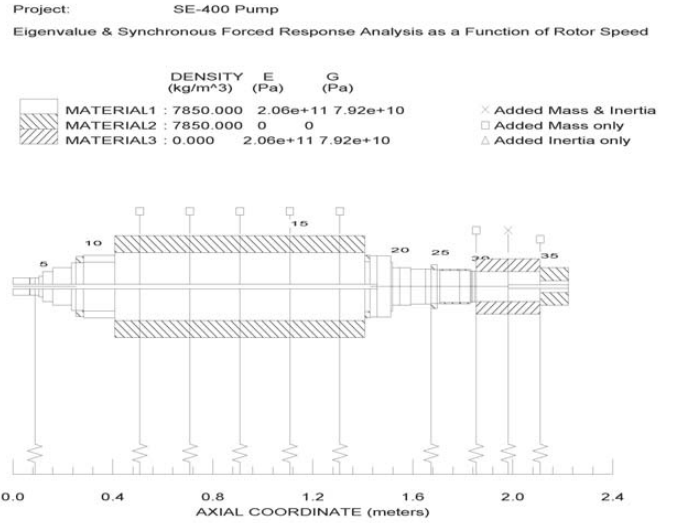


Figure 3. Submerged Motor/Pump Rotordynamic Model.

referred to as the Bernoulli effect. When circulating the oil internally in the motor, axial velocities in the clearance give rise to another effect called the Lomakin effect, which acts as a stabilizing, positive direct stiffness effect. The resulting stiffness in the fluid filled rotor clearance space is dependent on the relative influence from these two effects. However, common for the large submerged motors discussed here is domination of the circumferential Bernoulli effect, giving a large added mass and negative stiffness.

The damping has also shown to contribute significantly to the rotordynamic behavior of the fluid filled rotor/stator clearance. As presented by Black (1979), the damping is inversely proportional to $(C_r/R)^3$ and directly proportional to the rotor length.

Typical for the response of a submerged motor is that the critical speed is reduced significantly by both the added mass and negative stiffness. The fundamental bending mode shapes also become generally well damped, as shown by White, et al. (1992).

In this analysis, rotordynamic coefficients for the motor clearance were analyzed by two different approaches: Black’s simplified equations and models based on the bulk flow presented by Childs (1993), also discussed by Storteig (2000). The bulk flow models can be used for both short and long clearances but the basic theory assumes turbulent flow, typically found in annular seals with high differential pressures (axial Reynolds number $Re_a > 5$ to 10,000). The simplified Black model assumes laminar or vortex flow and no axial throughflow. In Table 3, a listing of the submerged rotor coefficients is presented, using a submerged reference mass $M_{addref} = (\rho_{fluid} \cdot R^2 L)$. In the present rotor analysis, the coefficients based on the bulk flow model were used, although the Bernoulli effect will be by far the most significant effect, giving a large negative stiffness. What should be noticed, however, is the significant damping present in the clearance.

Table 3. Oil Filled Rotor/Stator Clearance Rotordynamic Coefficients, Reference Mass: $M_{addref} = (\rho_{fluid} \cdot R^2 L)$ (kg).

Rotordynamic coefficients	Dimension	Bulk flow model	Black
$K/(M_{addref} \omega^2)$	[-]	-16.70	-28.22
$k/(M_{addref} \omega)$	[1/s]	4692	7693
$C/(M_{addref})$	[1/s]	9379	15386
$c/(M_{addref} \omega)$	[-]	67.72	112.89
$M/(M_{addref})$	[-]	67.72	112.89

Unbalanced Magnetic Pull, UMP

There will exist a magnetic destabilizing force (negative stiffness) acting on a rotor, which is eccentric in the motor clearance. Several early publications present the effect on the shaft critical speed, as discussed by von Kaehne (1963). This phenomenon in electric motors should always be taken into account in the rotordynamic analysis, although the exact representation can be difficult to achieve. However, the basic representation is given in the following, simplified for small eccentricities, as presented by Wright, et al. (1982):

$$K_{ump} = Q_{ump} \cdot \frac{\pi}{4} D \cdot l \cdot B^2 \frac{1}{C_r \cdot \mu_0} \quad (2)$$

where:

D = Rotor diameter (m)

l = Rotor length (m)

B = Peak flux density, concentric condition (Tesla)

C_r = Air gap radial clearance (m)

μ_0 = Magnetic permeability of free space (Henry/m)

Q_{ump} = Pole number factor

The constant Q_{ump} is usually dependent on the pole number, meaning higher force for higher pole numbers. For simplicity, K_{ump} was assumed to be independent of running speed.

Bearings

The bearing at the nondrive-end (NDE) is of a cylindrical roller design that supports radial loads. At the drive-end (DE), the combination of a large spherical roller bearing and tapered roller bearing supports both axial and radial loads. The axial thrust in the submerged pump is balanced to give a defined net force downward, i.e., toward the suction side of the impeller. This gives a stable tension in the shaft and ensures a well defined axial thrust direction on the spherical roller bearing.

The roller bearings typically have high radial stiffness and very low damping. The damping is often neglected for rotordynamic analysis. The radial stiffness was calculated using commercially available software.

Impeller and Seals

The impeller is of a mixed flow design giving rise to significant fluid interaction forces. The wear ring seal rotordynamic coefficients were calculated using the bulk flow model, as presented by Childs (1993). The interactions in terms of stiffness and damping are essential for the impeller overhung dynamics.

The impeller/diffuser interaction in a centrifugal pump is discussed by several authors and a comparison of different results is carried out by Childs (1993) and Brennen (1994). Torbergsen and White (2000) have presented results for a radial impeller in an axial diffuser. The radial design was only analyzed with regard to impeller/diffuser interactions and the test configuration had a minor influence from the front shroud clearance. It was decided in this analysis to compare different measured coefficients in order to investigate the effect on the global rotordynamic analysis. A mixed flow impeller in an axial diffuser will see interaction from the axial diffuser design as presented by Torbergsen and White (2000) and the front shroud clearance, as included in other published impeller results.

In Table 4, the impeller wear ring details are shown. In the analysis, only nominal clearances were considered in the rotordynamic analysis. A comparison of measured impeller interaction coefficients (dimensionless) is presented in Table 5, based on Torbergsen and White (2000) and a volute configuration presented by Brennen (1994). The coefficients are based on flows near the best efficiency point (BEP).

From the above comparison it can be seen that the negative stiffness is much higher for the impeller discussed in Brennen

Table 4. Impeller Wear Ring Parameters for Calculating Seal Dynamic Coefficients.

Description	Data impeller front space seal	Data impeller back space seal
Seal clearance ratio C_r/R [-]	0.0015	0.0015
Dynamic fluid viscosity [cP]	1	1
Seal pressure drop Δp [bar]	4.5	3.5
Relative inlet swirl	0.6	0.6

Table 5. Dimensionless Rotordynamic Coefficients for an Impeller Whirling in a Diffuser or Volute.

Impeller coefficients [-]	Made dimensionless by	Torbergsen impeller	Brennen impeller
K	$\rho \pi^2 b_2 \omega^2$	-0.4	-2.65
k	$\rho \pi^2 b_2 \omega^2$	0.5	1.04
C	$\rho \pi^2 b_2 \omega$	1.7	3.8
c	$\rho \pi^2 b_2 \omega$	3.6	8.96
M	$\rho \pi^2 b_2$	5.7	6.6
m	$\rho \pi^2 b_2$	0	-0.903

(1994). Impeller stiffness will always be negative due to the earlier mentioned Bernoulli effect, in the same way as for the long submerged rotor. However, the negative stiffness is only on the order of 1 MN/m or less, which is lower than other interactions occurring along the rest of the rotor and will therefore not contribute significantly to the overall dynamics.

The impeller cross-coupled stiffness is in the same way as for wear ring seals, important for the overall response and stability. The higher stiffness from the impeller discussed in Brennen (1994) is most probably due to the influence from the front shroud clearance. Other authors have also shown this effect to contribute significantly. The impeller damping and added mass, however, will contribute much more to the overall dynamic behavior of the pump.

Rotor Core Stiffness

The motor rotor core will increase the shaft stiffness by a certain fraction of the motor core area moment of inertia. For the actual case, free-free resonance tests were carried out to study the core stiffening effect. For submerged rotors, the core is modeled as an equivalent shaft diameter giving the same stiffness as deduced from measurements of the fundamental natural frequency.

Rotordynamic Analysis

The rotor imbalance was applied according to balancing grade G2.5. An evaluation of the hydraulic imbalance for the impeller has also been carried out. For cast impellers, this will be higher than the mechanical imbalance. Verhoeven (1988) reported a hydraulic unbalance in the range of K_{HI} 0.02 to 0.12 for sand casted impellers, where K_{HI} is referred to as the hydraulic unbalance force coefficient. The casting process applied here is precision cast so the lower value $K_{HI} = 0.02$ was applied but still considered conservative for the analysis.

Sample calculations using both impeller coefficients discussed in Brennen (1994) and Torbergsen and White (2000), showed no significant differences in the results in the range of interest. However, the results presented here are based on Brennen (1994) coefficients in order to obtain a conservative estimation (higher added mass and negative stiffness).

From the eigenvalues, a first natural frequency is detected at 1966 cpm when operating at the nominal speed $n = 985$ rpm, with the mode shape as shown in Figure 4. The critical damping ratio is 0.27, which is considered as critically damped according to API 610, Eighth Edition. This mode shape is related to the motor rotor with highest response at the center of the motor. The second mode shape of interest is shown in Figure 5 and is related to the impeller overhang critical. It can be seen that the natural frequency is well above and away from any speed of interest (3768 cpm) although

the damping ratio is low (0.088). In Figure 6, the result from a forced response analysis is shown, with a speed range up to 4000 rpm, which is much higher than any speed typically applied to this type of design. The impeller and motor rotordynamic coefficients were calculated over the whole range. The response values are very low at the operating speed, $40 \mu\text{m}$ peak-to-peak for the motor and approximately $100 \mu\text{m}$ peak-to-peak in vibration response for the lower wear ring seal position. This is much lower than the applied wear ring seal diametrical clearances (<math><15\text{ percent}</math>). The possibility for impeller wear ring seal touch and wear is thus very low. This conclusion is also in accordance with experience from various SE pumps.

ROTORDYNAMIC MODE SHAPE PLOT
Project: SE-400 Pump
Eigenvalue & Synchronous Forced Response Analysis as a Function of Rotor Speed
ANALYSIS POINT: ROTOR SPEED = 985 (RPM)
NAT FREQ = 1966 cpm, DAMPING RATIO = 0.272, POTENTIAL SYNC CRIT SPEED = 2328
STATION 12 ORBIT FORWARD PRESSION

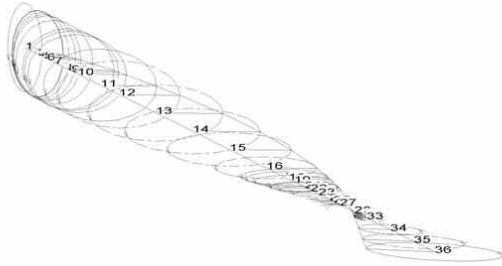


Figure 4. First Mode Shape, Motor Rotor, with Natural Frequency 1966 CPM (Forward Precession). Impeller side to the right and motor core to the left.

ROTORDYNAMIC MODE SHAPE PLOT
Project: SE-400 Pump
Eigenvalue & Synchronous Forced Response Analysis as a Function of Rotor Speed
ANALYSIS POINT: ROTOR SPEED = 985 (RPM)
NAT FREQ = 3768 cpm, DAMPING RATIO = 0.088, NO SYNC CRIT SPEEDS IN RANGE
STATION 36 ORBIT FORWARD PRESSION

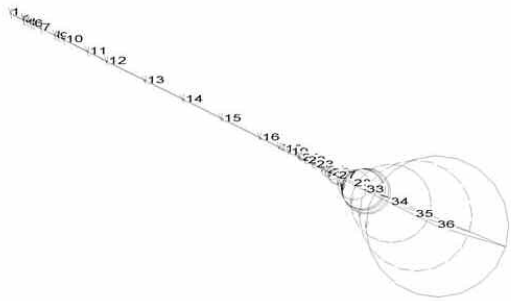


Figure 5. Second Mode Shape, Impeller Overhang, with Natural Frequency 3768 CPM (Forward Precession). Impeller side to the right and motor core to the left.

HYDRAULIC DESIGN

The actual impeller/diffuser design was developed using traditional one-dimensional methods together with inhouse references for similar designs. The use of similarity and affinity laws and specific speeds often forms the basis when going to larger capacities. Although the use of numerical simulations in turbomachinery design has become common, basic pump design with one-dimensional analysis will still be important.

A mixed flow impeller combined with an axial diffuser leads to the impeller/diffuser interactions being an important issue, not only for the rotordynamic behavior but also for head flow stability. At off-design it is quite common for the diffuser to recirculate but if the recirculation propagates around the circumference periodically this makes the flow through the diffuser unstable. Several articles

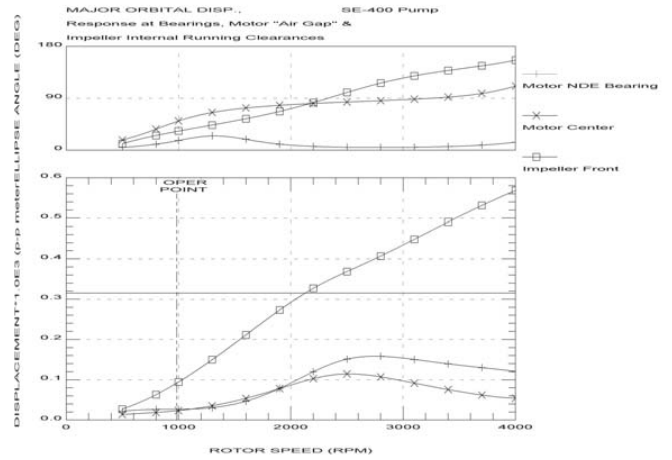


Figure 6. Bode (Harmonic Analysis Response) Plot Showing Dynamic Response at Different Operational Speeds. Actual operating speed = 985 rpm.

discuss axial diffuser rotating stall influence on both performance and shaft excitational forces, for both pumps and compressors. Typical for axial diffuser pumps are rotating stall frequencies of <math><10\text{ percent}</math> of shaft rotational speed, i.e., very low frequency. The hydraulic performance can be heavily influenced by these phenomena. The head-flow characteristic can show a hysteresis around the flow at the onset of stall, depending on an increase or decrease of the flow when approaching the onset capacity.

Additionally, shaft forces and vibration can occur at low frequency. This has been presented by Torbergsen and White (1998) for a radial impeller in an axial diffuser. General design methods for avoiding this have been published but few with relations to centrifugal pumps. An axial diffusion factor, D_f for the diffuser, can be applied based on the theory presented by Leiblein (1965) and discussed by Greitzer (1981) and Brennen (1994). This is describing the ratio of area development in an axial cascade of blades.

$$D_f = 1 - \frac{\sin \beta_3}{\sin \beta_4} + \frac{\sin \beta_3 (\cot \beta_3 - \cot \beta_4)}{2s} \quad (3)$$

where β_3 and β_4 diffuser inlet and outlet angles and s is vane cascade solidity. The references discuss the possibility of diffuser stall if the D_f is above 0.6. In many practical cases, for axial diffusers in pumps, this can be hard to achieve. But the diffusion factor should be kept as low as possible. However, inhouse experience has also shown several designs with higher diffusion factors without any instability problems. Typically, $D_f < 0.8$ can be acceptable in some cases, especially for lower specific speeds, $n_q < 30$.

This is not the only parameter that should be considered and experience has shown that there is need for more research to fully control the axial diffuser rotating stall phenomenon. One important factor is the area ratio between the impeller outlet and diffuser inlet. Experience shows a higher possibility of rotating stall if the impeller/diffuser area ratio is too high. However, as will be shown, transient numerical simulations are capable of detecting any sign of propagating flow instabilities in the diffuser.

In Table 6, the main parameters for the present design are listed.

NUMERICAL ANALYSIS

To verify pump characteristic and hydraulic stability, extended numerical flow simulations (CFD) were carried out. This involves steady-state and fully transient simulations. By using a commercial CFD-code, advanced modeling techniques, and computer time, any off-design flow instability, including head-flow hysteresis, is possible to simulate and study. The low frequency of these

Table 6. Impeller and Diffuser Design Parameters.

Design parameter	Design data
Impeller diameter[mm]	825 (32.5 in)
Outlet width[mm]	106 (4.2in)
Outlet blade angle (β_2)	25
No. of impeller blades	6
No. of diffuser vanes	11
Diffuser solidity	2.7
Diffusion factor of axial diffuser (D_f)	0.67

phenomena makes the simulation very time consuming. Simulation and measurements of instabilities are discussed and presented by Torbergsen and White (1998) for a submerged pump with an axial diffuser. Inhouse experience has also shown that such instabilities can be detected by transient CFD simulations.

The numerical modeling and simulations were carried out using a Reynolds averaged Navier-Stokes finite volume code, including a shear stress transport model for turbulence modeling and logarithmic wall functions for the flow in low Reynolds number regions near a solid wall. The boundary conditions are applied to the inlet as constant pressure and outlet as constant mass flow rate. Special focus was on the outlet boundary to ensure that the outlet boundary had no influence on the upstream diffuser flow, that is, the boundary had to be placed in a sufficient distance to the diffuser. The combined impeller/diffuser numerical model is shown in Figure 7. For more details about the theoretical and numerical modeling, refer to Ansys CFX (2004).

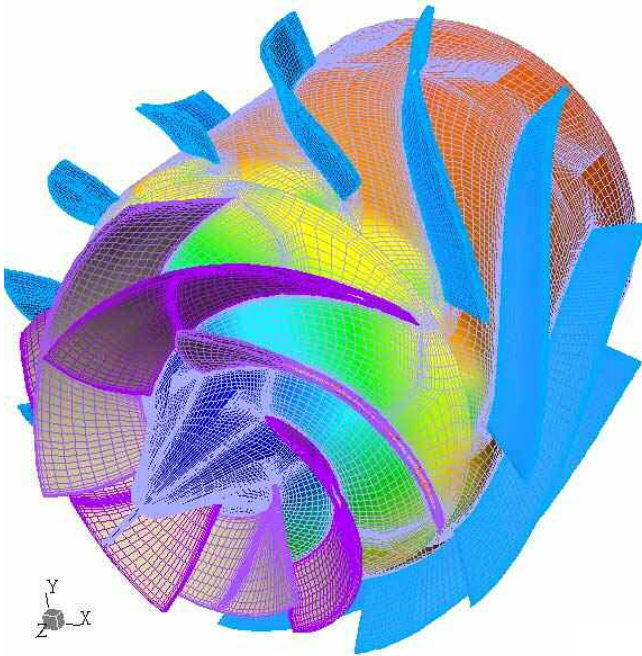


Figure 7. 3D CFD Model of the Combined Impeller and Diffuser.

FLOW SIMULATIONS AND PROTOTYPE TEST RESULTS

The steady-state characteristic of the present submerged pump case is shown in Figure 8, together with the final measured characteristic from the full scale test. The volumetric losses in the wear ring seals were corrected in the whole flow range in order to give realistic flows in the simulations. The simulations show good agreement with the results from the actual inhouse test. However, as expected, at the lowest capacities, a small difference can be seen. Off-design simulations are often more difficult to carry out

due to severe flow separation and transient behavior. It is of special importance to place the boundary conditions in sufficient distance from any flow separation, i.e., the outlet boundary is often critical at low flow simulations.

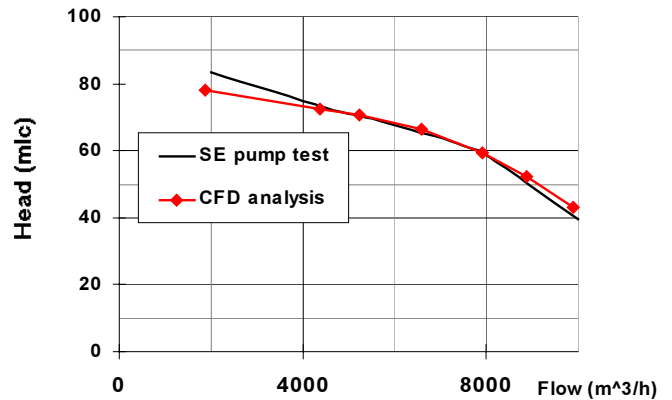


Figure 8. Numerical Simulation of Flow Head Characteristics, Together with Test Points for the Actual Pump.

The shaft power consumption and efficiencies are shown in Figure 9. Both test and simulated values are included. The impeller torque was calculated by the use of CFD simulations with integrated pressure and shear forces along the blades and shrouds. However, the disk friction in the front and back leakage paths and wear ring volumetric and friction losses have to be calculated manually, based on known methods as presented in Lazarkiewicz and Trokolanski (1965) and bulk flow models.

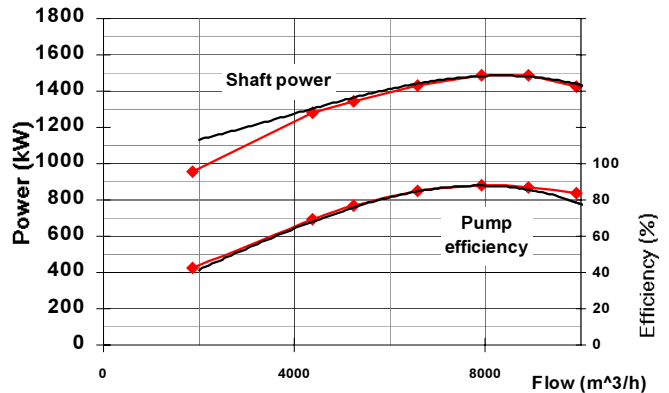


Figure 9. Numerical Simulation of Shaft Power and Efficiency (Red Marks), Together with Test Curve Actual Pump. Front and back friction and volumetric losses included in the calculated values.

Enhanced transient simulations were carried out over the whole flow domain, showing no onset of rotating stall in the 30 to 150 percent region. An example of the off-design simulation is shown in Figure 10. Reversed axial velocities are shown as colors, indicating the recirculation zones at the diffuser vane suction sides. In case of diffuser instability, whole channels are blocked periodically (Torbergsen and White, 1998). The blocked stall zone will then propagate circumferentially around the diffuser. However, it can be seen that the zones are quite stable for both time steps with open flow passages for throughflow in each channel. The boundary conditions were varied in order to simulate increase and decrease of the flow, which means the same as opening and closing of a throttle valve in the case of full scale testing. The objective was to detect any hysteresis on the flow-head characteristic as discussed earlier. No sign of periodic instability causing hydraulic and dynamic problems was present. This is in accordance with the observed head capacity characteristic from full scale testing. A dense flow registration with both opening and closing of the valves showed no flow hysteresis.

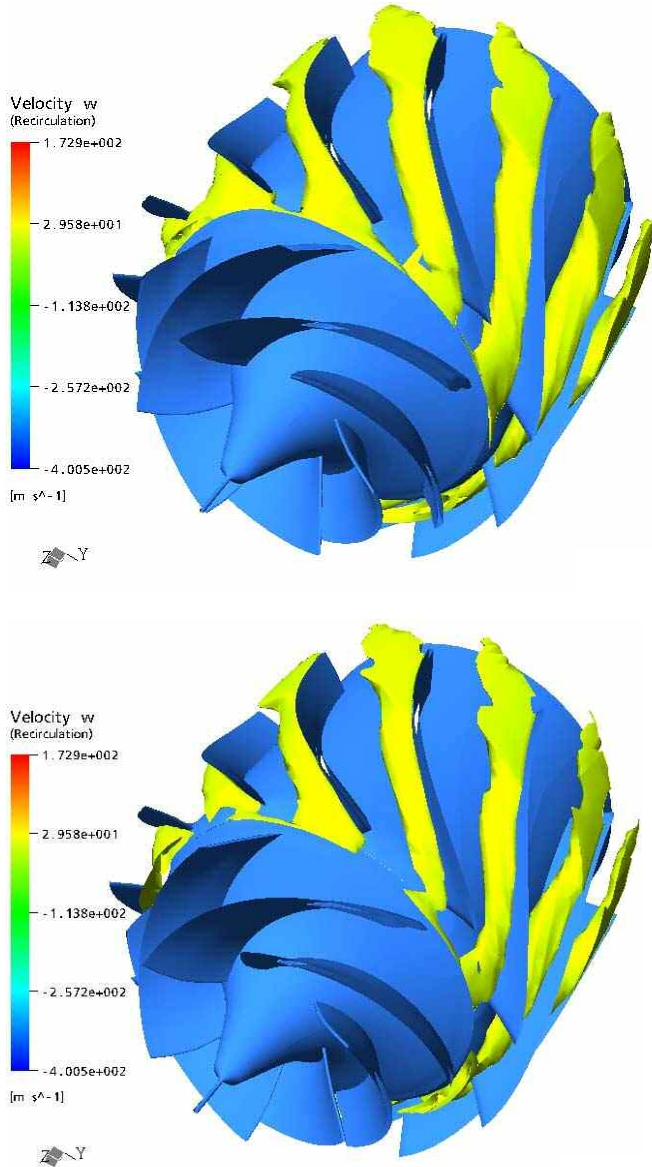


Figure 10. Numerical Simulations of Flow at Off-Design/Part Load. Two different time steps showing diffuser channel recirculation (5/4 revolutions between the time steps, isosurfaces of reversed axial velocities). Stable recirculation zones in terms of circumferential propagation (no rotating stall instability).

To further confirm the stability during testing, vibration measurements were used. Earlier published articles discuss the use of a blade stall interaction frequency to detect the onset capacity and strength of rotating stall (Torbergsen and White, 1998). A distinct blade-stall interaction frequency, $f_{bladestall}$, often slightly lower than the blade passing frequency, but at greater amplitude, is present in the unstable region, as shown in Equation (4):

$$f_{bladestall} = n \cdot (f_{impeller} - f_{stall}) \quad (4)$$

where n is the number of impeller blades and f_{stall} is the stall propagation frequency. Experience has also shown that a distinct correlation exists between hydraulic instability and blade passing interactions and this can be detected by casing or bearing house vibrations.

In the present case, with a propagation frequency of between 5 and 10 percent of the rotating speed, the blade passing frequency typically would shift from approximately 99 Hz to 88 to 93 Hz. In

Figure 11, the radial vibration measured at the pump casing close to the guide vanes and bearing bracket is shown for rated capacity and 30 percent flow. At off-design, no distinct blade passing interaction is seen, confirming the hydraulic stability down to at least 30 percent flow, while the blade passing at 99 Hz is seen at rated flow. The vibration level is below 2 mm/s at rated flow but increases to approximately 4 mm/s at 30 percent flow. The $1\times$ component at 16.5 Hz is low for both flows (<1 mm/s), confirming low response to imbalance, as indicated in the rotordynamic analysis. Figure 12 shows total radial vibration level for different flow rates, showing lowest vibration level around BEP (<2 mm/s).

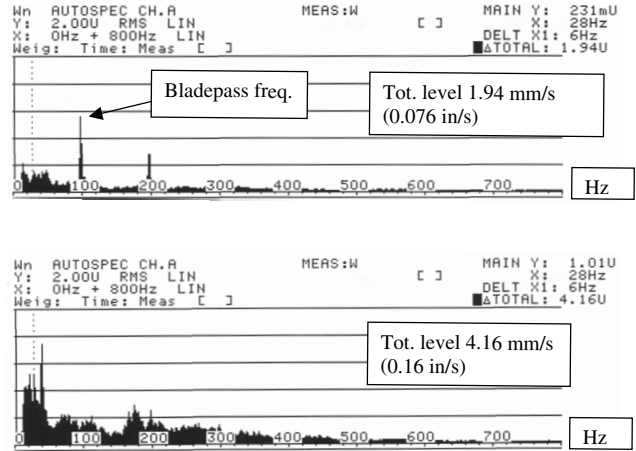


Figure 11. Casing/Bearing House Radial Vibrations at Rated Capacity (Top) and 30 Percent Flow (Bottom).

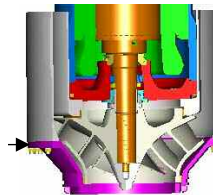
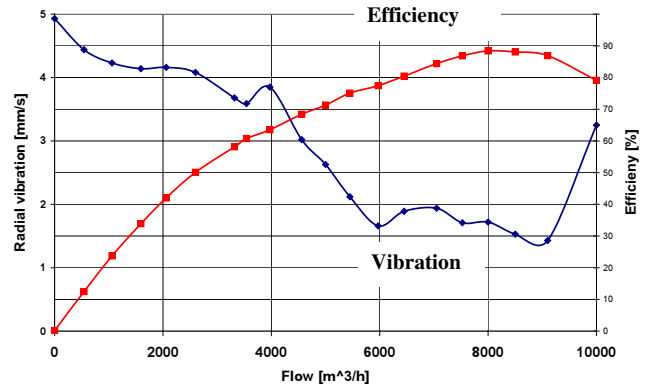


Figure 12. Radial Casing/Bearing House Vibrations Versus Flow Compared with the Efficiency, 10 to 1000 Hz.

The above discussion is an important part of the full scale testing of submerged electric pumps. Although the shaft relative vibration is difficult to measure, necessary information regarding performance and dynamics can be gathered by using casing vibration analysis.

CONCLUSIONS

A submerged electric pump for high capacities (65 mlc at 7000 m³/h) has been analyzed and tested. Based on the main challenges for this pump type, the following conclusions have been made:

- The torsional analysis showed a quasistatic response to torsional excitation at direct online start up.
- The first lateral bending mode was related to the motor itself. The separation margin was 100 percent, that is, the mode was at $2\times$ the operational speed at 985 rpm. The response was highly damped. The impeller overhung mode was located at even higher speeds. The forced response showed peak-to-peak values below 15 percent of the wear ring seal clearances.
- Hydraulic analysis was carried out using numerical simulations (CFD). The diffuser stability has been focused and no diffuser rotating stall was observed in the flow domain of interest.
- Additional test measurements were carried out on the full scale pump and low vibration values were observed, as expected from the rotordynamic analysis. No sign of blade-stall interaction frequencies was observed, confirming diffuser stability at both rated flow and off-design. Additional dense head-flow analysis at off-design confirmed the stable performance.

The above points will form the basis for submerged electric pumps when increasing the flow domain even more.

NOMENCLATURE

B	= Flux density
b_2	= Impeller outlet width
C	= Direct damping [Ns/m] or [-], or clearance
c	= Cross-coupled damping [Ns/m] or [-]
D	= Rotor diameter [m]
f	= Frequency [Hz]
H	= Head [mlc]
I	= Polar moment of inertia [kg m ²]
K	= Direct stiffness [N/m] or [-]
K_{HI}	= Hydraulic imbalance factor
k	= Cross-coupled stiffness [N/m] or [-]
l	= Rotor length [m]
M	= Added mass/inertia coefficient [kg] or [-]
M_{addref}	= Submerged rotor reference mass $\rho_{\text{fluid}} R^2 L$ [kg]
m	= Cross-coupled inertia coefficient [kg] or [-]
P	= Motor rating maximum power [kW]/[hp]
p	= Pressure [bar]
Q	= Flow rate or pole number factor [-]
r_2	= Impeller outlet radius
s	= Vane cascade solidity (= vane cord length/circumferential vane distance)
T	= Motor torque, rated or transient [Nm]
BEP	= Best efficiency point
NPSHr	= Net positive suction head required [m]/[ft]
β	= Blade/vane angle [degree]
ϕ	= Phase angle [degree]
τ	= Time constant [1/s]
μ_0	= Magnetic permeability of free space [Henry/m]
ω	= Angular frequency of rotation [rad/s]
ρ	= Density
Ω_n	= shaft speed [rpm]

Subscripts

S	= Any variable
S_2	= Impeller outlet
S_3	= Diffuser inlet
S_4	= Diffuser outlet
S_i	= Counter
S_r	= Radial
S_n	= Nominal or rated

REFERENCES

- Ansys CFX, 2004, "User Manual," Ansys Inc.
- Brennen, C. E., 1994, *Hydrodynamics of Pumps*, Oxford, United Kingdom: Oxford University Press.
- Black., H. F., 1979, "Effects of Fluid-Filled Clearance Spaces on Centrifugal Pump and Submerged Motor Vibrations," *Proceedings of the Eighth Turbomachinery Symposium*, Turbomachinery Laboratory, Texas A&M University, College Station, Texas, pp. 29-34.
- Greitzer, E. M., 1981, "The Stability of Pumping Systems," *ASME Journal of Fluids Engineering*, pp. 193-242.
- Childs, D. W., 1993, *Turbomachinery Rotordynamics*, New York, New York: John Wiley & Sons.
- Lazarkiewicz, S. and Troskolanski, A. T., 1965, *Impeller Pumps*, Oxford, United Kingdom: Pergamon Press Ltd.
- Lieblein, S., 1965, "Experimental Flow in Two-Dimensional Cascades," Chapter 6, *Aerodynamic Design of Axial Flow Compressors*, NASA SP-36.
- Storteig, E., 2000, "Dynamic Characteristics and Leakage Performance of Liquid Annular Seals in Centrifugal Pumps," Doctoral Thesis, Norwegian University of Science and Technology, Department of Marine Engineering.
- Torbergsen, E. and White, M. F., 1998, "Diffuser Rotating Stall and Influence on Shaft Excitatory Forces, Part 2: Numerical Investigation," *Proceedings of International Symposium on Computational Technologies for Fluid/Thermal/Structural/Chemical Systems with Industrial Applications*, ASME-PVP, pp. 41-49.
- Torbergsen, E. and White, M. F., 2000, "Rotordynamic Interaction of a Centrifugal Pump Impeller in an Axial Diffuser," *IMEchE Proceedings of Vibrations in Rotating Machinery*, pp. 679-690.
- Verhoeven, J. J., 1988, "Rotordynamic Considerations in the Design of High Speed, Multistage Centrifugal Pumps," *Proceedings of the Fifth International Pump Users Symposium*, Turbomachinery Laboratory, Texas A&M University, College Station, Texas, pp. 81-92.
- von Kaehne, P., 1963, "Unbalanced Magnetic Pull in Rotating Electric Machines," ERA Report Z/T142.
- White, M. F., Torbergsen, E., Jacobsen, O. H., and Lumpkin, V. A., 1992, "Dynamic Analysis of the Motor for a Downhole Electric Submersible Pump," *IMEchE Proceedings of Vibrations in Rotating Machinery*, pp. 499-508.
- Wright, M. T., Gould, D. S. M., and Middlemiss, J. J., 1982, "The Influence of Unbalanced Magnetic Pull on the Critical Speed of Flexible shaft Induction Machines," *Proceedings of International Conference on Electrical Machines—Design and Applications*, IEEE Conference Pub. No. 213, pp. 61-64.